

## ARTICLE

# Structural and chemical properties of half-sandwich rhodium complexes supported by the bis(2-pyridyl)methane ligand

Davide Lionetti,<sup>a</sup> Victor W. Day,<sup>a</sup> and James D. Blakemore<sup>\*a</sup>Received 00th January 20xx,  
Accepted 00th January 20xx

DOI: 10.1039/x0xx00000x

[Cp\*Rh] complexes (Cp\* = pentamethylcyclopentadienyl) supported by bidentate chelating ligands are a useful class of compounds for studies of redox chemistry and catalysis. Here, we show that the bis(2-pyridyl)methane ligand, also known as dipyridylmethane or dpma, can support [Cp\*Rh] complexes in the formally +III and +II rhodium oxidation states. Specifically, two new rhodium complexes ([Cp\*Rh(dpma)(L)]<sup>+</sup>, L = Cl<sup>−</sup>, CH<sub>3</sub>CN) have been isolated and structurally characterized, and the properties of the complexes have been compared with those of [Cp\*Rh] complexes bearing the related dimethyldipyridylmethane (Me<sub>2</sub>dpma) ligand. Complex [Cp\*Rh(dpma)(NCCH<sub>3</sub>)]<sup>2+</sup> displays a quasireversible rhodium(III/II) reduction by cyclic voltammetry; related electron paramagnetic resonance (EPR) spectroscopic studies confirm access to the unusual rhodium(II) oxidation state. Further reduction to the formally rhodium(I) oxidation state, however, is followed by deprotonation of dpma, as observed in electrochemical studies and chemical reduction experiments. This reactivity can be understood to occur as a consequence of the presence of doubly benzylic protons in the dpma ligand, since use of the analogous Me<sub>2</sub>dpma enables reduction to rhodium(I) without involvement of ligand deprotonation. These findings highlight the important role of the ligand backbone substitution pattern in influencing the stability of highly-reduced complexes, a key class of metal species for study of electron and proton management in catalysis.

## 1. Introduction

Half-sandwich rhodium complexes supported by chelating bidentate ligands are appealing for study of electron transfer and proton management during reductive catalysis, as they can be prepared by straightforward synthetic routes, are built upon readily available precursor materials, and often quite stable in the Rh(III) oxidation state. In recent years, [Cp\*Rh] complexes have attracted increased attention for mechanistic and structure-function studies of the hydrogen (H<sub>2</sub>) evolution reaction, an important transformation in energy science,<sup>1–3</sup> as well as for use in industrial settings as catalysts for the regeneration of nicotinamide coenzymes.<sup>4</sup> In important early work from Kölle and Grätzel, [Cp\*Rh(bpy)]<sup>2+</sup> (bpy = 2,2′-bipyridyl) was demonstrated to be a robust electrocatalyst for H<sub>2</sub> generation from H<sub>2</sub>O.<sup>5,6</sup> Steckhan and coworkers found that the system was also active for hydrogenation of biological cofactors (e.g., NAD<sup>+</sup>, NADP<sup>+</sup>) using formate (HCO<sub>2</sub><sup>−</sup>) as a reductant,<sup>7,8</sup> leading to applications of this catalyst in bioelectrochemical cells.<sup>9,10</sup> More recently, mechanistic studies by our group<sup>11</sup> as well as by Miller and coworkers<sup>12</sup> have revealed that the Cp\* ligand, traditionally viewed an “innocent” ancillary ligand, can be directly involved in proton transfer and act as a pendant base during protonation of rhodium(I) species.

This behavior has enabled the preparative-scale isolation and spectroscopic and structural characterization of uncommon pentamethylcyclopentadiene ([Cp\*H]) complexes supported by bpy and related α-diimine ligands.<sup>13</sup> As these compounds are prepared under conditions relevant to H<sub>2</sub> evolution catalysis and evolve H<sub>2</sub> upon protonation, their direct involvement in chemistry leading to H<sub>2</sub> is likely.<sup>14</sup>

Prompted by these findings, our group has recently initiated studies of a variety of previously unexplored [Cp\*Rh] compounds supported by bidentate chelates beyond the common 2,2′-bipyridyl ligand (Chart 1). In general, we have found that the nature of the bidentate ligand plays a key role in determining the reactivity profiles of these systems in electron- and proton-transfer processes. Catalytic activity is retained and similar [Cp\*H] intermediates are observed upon introduction of substituents on the bpy framework,<sup>13,14</sup> with the exception of strongly electron-withdrawing nitro (–NO<sub>2</sub>) groups, which engender more dramatic changes in reactivity.<sup>15</sup> On the other hand, replacement of one or both pyridine donors with phosphine moieties affords access to more traditional and isolable metal–hydride species upon protonation of reduced precursor complexes and, importantly, concurrent loss of electrocatalytic H<sub>2</sub> evolution activity.<sup>16–18</sup>

Adding further diversity to this area, we have recently been exploring the chemistry of [Cp\*Rh] complexes supported by the Me<sub>2</sub>dpma ligand<sup>19</sup> (dpma = bis(2-pyridyl)methane, often identified as dipyridilmethane in the literature;<sup>20</sup> Me<sub>2</sub>dpma = dimethylbis(2-pyridyl)methane)). Me<sub>2</sub>dpma is a bidentate chelating ligand that features two unconjugated pyridine donors linked by a –C(CH<sub>3</sub>)<sub>2</sub>– bridge.<sup>19</sup> The [Cp\*Rh] complexes

<sup>a</sup> Department of Chemistry, University of Kansas, 1567 Irving Hill Road, Lawrence, Kansas 66045, USA. E-mail: blakemore@ku.edu; Tel: +1 (785) 864-3019.

<sup>†</sup> Electronic Supplementary Information (ESI) available: Spectroscopic (NMR, UV-Vis), electrochemical, and crystallographic (XRD) data. See DOI: 10.1039/x0xx00000x

of Me<sub>2</sub>dpma possess unique electrochemical properties, in that two sequential one-electron transfer steps are observed in cyclic voltammetry experiments, corresponding to the Rh(III)/Rh(II) and Rh(II)/Rh(I) couples of [Cp\*Rh(Me<sub>2</sub>dpma)(NCCH<sub>3</sub>)]<sup>2+</sup>. This is an unusual behavior in this class of compounds, as most [Cp\*Rh] complexes display net two-electron voltammetric profiles that indicate rapid formation of Rh(I) upon reduction of Rh(III).<sup>5,6</sup> As a result, the reductive chemistry of most [Cp\*Rh] complexes is dominated by disproportionation of transient Rh(II) complexes.<sup>6</sup> To our surprise, however, chemical preparation of the one-electron reduced species in our study revealed a possible role of the Me<sub>2</sub>dpma scaffold in stabilizing the Rh(II) complex.<sup>19</sup>

Specifically, in the solid-state structure of this complex, obtained via single-crystal X-ray diffraction (XRD) methods, a marginally significant distortion of one of the backbone methyl substituents on Me<sub>2</sub>dpma was observed, suggesting a possible interaction between the basic Rh(II) center and one of the methyl C–H bonds. Upon observation of this behavior, we became curious about the role of the methyl substituents of the Me<sub>2</sub>dpma ligand in engendering unique chemistry and have thus undertaken studies to explicitly probe the role of these ligand backbone substituents in tuning the structural properties and the electrochemical and chemical reactivity of the rhodium complexes in this family.

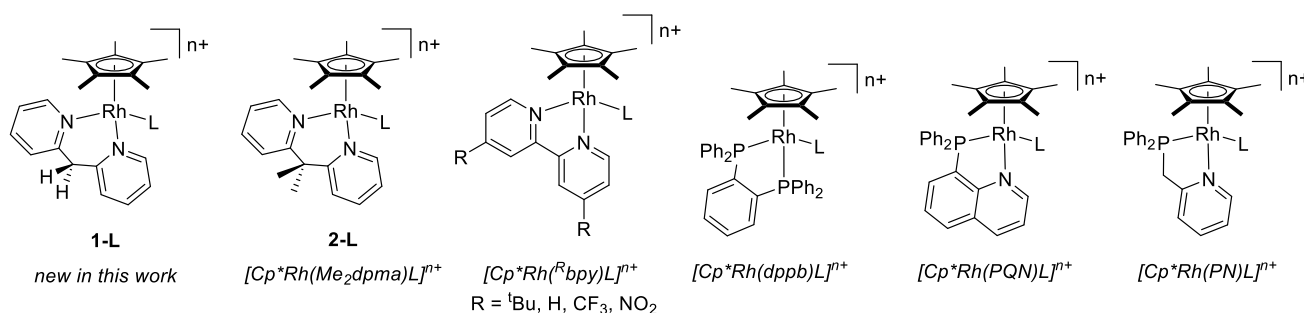


Chart 1. Rhodium half-sandwich complexes supported by bidentate ligand frameworks.

Here, we now report the synthesis and characterization of half-sandwich rhodium complexes bearing the dpma ligand, denoted **1-L** (Chart 1). The dpma ligand features a simple –CH<sub>2</sub>– bridge between two pyridine moieties, and therefore these complexes can be directly compared to others<sup>19</sup> supported by the Me<sub>2</sub>dpma ligand; complexes of dpma lack methyl groups at the bridging methylene position, and thus lack primary C–H bonds that could engage in direct interactions with the rhodium center upon reduction. Notably, there are only a limited number of available solid-state structures of complexes supported by the dpma ligand, including several for complexes of Cu<sup>21–26</sup> and Pt<sup>25,27–30</sup>, along with a limited number with other metals, including Pd,<sup>31</sup> Ru,<sup>32</sup> Hg,<sup>33</sup> Mo,<sup>34</sup> and Re.<sup>35</sup> However, no reports involving the solid-state structural characterization of rhodium complexes of the dpma ligand have thus far appeared in the literature,<sup>36</sup> and no [Cp\*Rh] complexes of this ligand platform have been reported in the literature. Furthermore, our interest in the lesser known dpma platform has been increased by reports of C–H bond activation and olefin hydroarylation reactivity enabled by this ligand in Pt systems.<sup>27–30</sup> In accord with these prior reports, we find that substitution of Me<sub>2</sub>dpma with dpma on the [Cp\*Rh] platform results in substantial structural and chemical reactivity changes.

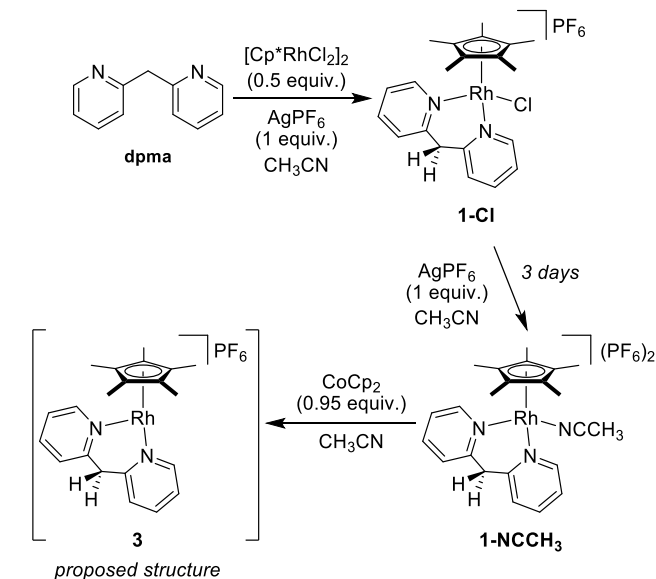
## 2. Results and Discussion

### Synthesis and Spectroscopic Characterization

Complex **1-Cl** was synthesized from Maitlis' useful [Cp\*RhCl<sub>2</sub>]<sub>2</sub> precursor<sup>37</sup> using a procedure similar to literature examples for analogous bidentate ligands (Scheme 1).<sup>14,16,17</sup> Abstraction of

one Cl<sup>–</sup> ligand per Rh center with AgPF<sub>6</sub>, removal of precipitated AgCl, and addition of the free dpma ligand afforded target complex **1-Cl** in near-quantitative yield. Characterization for **1-Cl** was obtained by nuclear magnetic resonance (NMR) methods. Complex **1-Cl** displays a set of four distinct resonances in the aromatic region of its <sup>1</sup>H NMR spectrum (δ 7.4–8.9 ppm), each integrating to two protons; these signals correspond to the four hydrogens on each of the two pyridine motifs (see Figure S1 in ESI). A singlet at 1.57 ppm, integrating to 15 H, is indicative of the Cp\* ligand, which rotates freely in solution. No three-bond coupling to the 100% abundance, NMR-active <sup>103</sup>Rh nucleus (*I* = 1/2) is observed in this resonance, but one-bond coupling to Rh is observed in the signal for the [Cp\*] ring carbons in the <sup>13</sup>C{<sup>1</sup>H} NMR spectrum (δ 97.82 ppm, d, <sup>1</sup>J<sub>C,Rh</sub> = 8.4 Hz; see Figure S2 in ESI).

Notably, the resonances corresponding to the hydrogens of the bridging CH<sub>2</sub> moiety on the dpma ligand appear as distinct doublets (δ 4.57 and 4.06 ppm); each set of peaks integrates to 1 H and displays significant splitting (15.5 Hz), indicative of geminal coupling. This appearance is reflective of the diastereotopic nature of the two protons on this methylene unit—while one proton is pointing toward the Cp\* ligand, the other points away from the [Cp\*Rh] fragment. To assign these two signals to the corresponding hydrogens, Nuclear Overhauser Effect Spectroscopy (NOESY) experiments were carried out. As shown in Figure 1, cross-peaks are observed between the doublet at 4.06 ppm and the singlet at 1.56 ppm (corresponding to the protons on Cp\*) and between the doublet at 4.57 ppm and one of the resonances in the aromatic region (δ 7.70 ppm), corresponding to protons on the pyridine moieties (see also Figure S7).



**Scheme 1.** Synthesis of half-sandwich rhodium complexes of the dpma ligand platform.

Given these observations, the resonances at 4.57 and 4.06 ppm can conclusively be assigned to the downwards- and upwards-facing protons, respectively, on the bridging methylene group (labelled H6A and H6B, respectively, in the XRD data, *vide infra*). The sharp resonances observed for the two protons on the bridging CH<sub>2</sub> moiety indicate that these two protons do not exchange readily on the NMR timescale, and that the complex displays C<sub>s</sub> symmetry in solution. Thus, exchange of the Cl<sup>−</sup> ligand (e.g. with CH<sub>3</sub>CN solvent molecules), which could activate a fluxional process resulting in reorientation of the bidentate dpma platform and, effectively, exchange of the two methylene protons, appears to be slow (or entirely inoperative) on the NMR timescale. This observation is in agreement with the solution behavior of the related [Cp\*Rh(Me<sub>2</sub>dpma)Cl][PF<sub>6</sub>] (**2-Cl**) complex, which displays distinct <sup>1</sup>H NMR signals (δ 2.06 and 1.89 ppm, s, 3H each) for the two methyl groups on the Me<sub>2</sub>dpma backbone.<sup>19</sup>

Treatment of **1-Cl** with 1 equiv. of AgPF<sub>6</sub> in CH<sub>3</sub>CN results in very gradual precipitation of colorless AgCl and in a concomitant lightening in solution color from orange to light yellow. Monitoring of reaction progress by <sup>1</sup>H NMR indicates slow conversion to a single new species containing both Cp\* and the dpma platform. After 3 days, the reaction was determined to be complete by NMR, the solution was filtered, and the volatiles were removed *in vacuo* to obtain **1-NCCH<sub>3</sub>** in quantitative yield. Characterization of **1-NCCH<sub>3</sub>** by <sup>1</sup>H NMR reveals a new set of resonances, shifted from those for **1-Cl**—four signals in the aromatic region (δ 7.5–8.8 ppm), each integrating to two protons and corresponding to the symmetric dpma framework, a singlet at 1.63 ppm (integrating to 15 H) corresponding to the Cp\* ligand, and two doublets at 3.91 and 4.62 ppm (<sup>2</sup>J<sub>H,H</sub> = 15 Hz) corresponding to the diastereotopic protons on the dpma methylene bridge (see Figures S8–S9 in ESI for spectra).

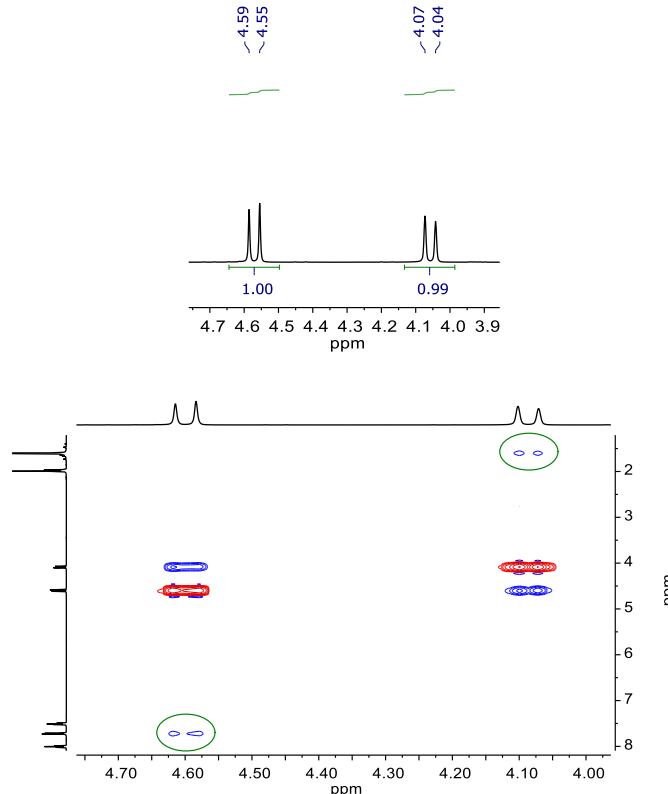


**Figure 1.** Upper panel: partial <sup>1</sup>H NMR (CD<sub>3</sub>CN, 500 MHz) of complex **1-Cl** displaying the resonances corresponding to the bridging methylene protons. Lower panel: partial NOESY spectrum (CD<sub>3</sub>CN, 500 MHz) of complex **1-Cl** highlighting the cross-peaks that indicate interactions between the bridging methylene protons and other sites in the complex (green dashed circles).

Notably, exchange of Cl<sup>−</sup> for CH<sub>3</sub>CN in the present system is substantially slower than in the case of **2-Cl**, as well as other complexes supported by similar bidentate ligands. In these other cases, the analogous reaction is essentially instantaneous and full conversion and precipitation of AgCl is usually observed within less than a minute. This difference in reactivity is a surprising consequence of substitution at the bridging position on the ligand framework and could result from the unique structural features of the dpma complexes **1-L** vs. those of their substituted analogues bearing Me<sub>2</sub>dpma (*vide infra*).

### X-Ray Diffraction Studies

The structural properties of the complexes **1-L** were assessed in the solid state via single-crystal X-ray diffraction (XRD) studies. Single crystals of **1-Cl** and **1-NCCH<sub>3</sub>** were grown via vapor diffusion of diethyl ether (Et<sub>2</sub>O) into a CH<sub>3</sub>CN solution of each compound. Successful crystallization of **1-NCCH<sub>3</sub>** is particularly gratifying given the difficulties commonly encountered in the solid state characterization of these solvento complexes, which tend to easily desolvate.<sup>19,38</sup> Both compounds crystallize in the *Pnma* space group; in each case, both the Rh-containing component and the outer-sphere PF<sub>6</sub><sup>−</sup> counteranion(s) are located on a crystallographic mirror plane. Atoms Rh1, C6, C7, C10, and Cl1 (**1-Cl**) or N3 (**1-NCCH<sub>3</sub>**) are located on the crystallographic mirror plane, which bisects the C9–C9A bond in

each complex. Thus, both complexes retain  $C_s$  symmetry in the solid state as well as in solution (*vide supra*).

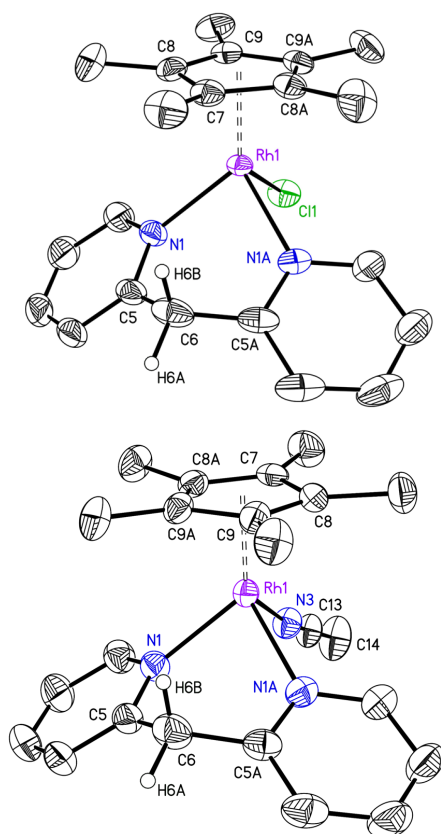


**Figure 2.** Solid-state structures (XRD) of **1-Cl** (upper structure) and **1-NCCH<sub>3</sub>** (lower structure). Displacement ellipsoids are shown at the 50% probability level. Hydrogen atoms (except for H6A and H6B) and outer-sphere  $\text{PF}_6^-$  counteranions are omitted for clarity.

In the solid state, the Rh centers in complexes **1-Cl** and **1-NCCH<sub>3</sub>** are six-coordinate, with the  $\text{Cp}^*$  ligand bound in the expected  $\eta^5$  fashion and the dpma platform bound in  $\kappa^2\text{-}[N,N]$  fashion in each case (Figure 2). The first coordination sphere at Rh is completed by a monodentate ligand—chloride in **1-Cl** and a  $\text{CH}_3\text{CN}$  solvent molecule in **1-NCCH<sub>3</sub>**. The cationic charges from the Rh(III)-containing components (+1 in **1-Cl**, +2 in **1-NCCH<sub>3</sub>**) are balanced by outer-sphere  $\text{PF}_6^-$  counteranions.

Due to the presence of the bridging methylene group, the dpma ligand enforces a six-membered metallocycle (vs. the five-membered metallocycle enforced by bpy and related ligands that lack this bridging group, Chart 1). Consequently, the bite angle of the dpma ligand (defined as the  $\text{N1-Rh1-N2}$  angle) is significantly larger ( $86.4(1)^\circ$ ) than the corresponding angle in literature bpy complexes ( $\approx 76^\circ$ ).<sup>39,40</sup> The dpma ligand in complex **1-NCCH<sub>3</sub>** displays a similarly wider bite angle ( $85.5(2)^\circ$ ). The metallocycles in **1-Cl** and **1-NCCH<sub>3</sub>** adopt a boat-like conformation, with Rh1 and C6 located on the same side of a plane defined by N1, C5, C5A, and N1A.

**Table 1.** Selected bond/plane distances and angle in **1-Cl**, **1-NCCH<sub>3</sub>**, and **2-Cl**.

	<b>1-Cl</b>	<b>1-NCCH<sub>3</sub></b>	<b>2-Cl</b> <sup>a</sup>
<i>Bond Distances (Å)</i>			
Rh1–N1	2.106(2)	2.106(3)	2.130(2); 2.129(2)
Rh1–N1A	2.106(2)	2.106(3)	2.133(2); 2.122(2) <sup>b</sup>
Rh1–C <sub>Cp*</sub> (avg.)	2.163	2.160	2.175; 2.175
Rh1–Cp* <sup>c</sup>	1.786	1.783	1.803; 1.803
Rh1–L	2.4078(8)	2.080(4)	2.4134(7); 2.4105(6)
	(L = Cl)	(L = CH <sub>3</sub> CN)	(L = Cl)
<i>Bond and Plane Angles (°)</i>			
N1–Rh1–N1A	86.4(1)	85.5(2)	85.44(8); 85.58(8) <sup>d</sup>
C5–C6–C5A	115.9(3)	117.2(4)	110.7(2); 111.5(2) <sup>e</sup>
Cp*–(N1–Rh1–N1A) <sup>f</sup>	60.5	56.1	67.4; 66.8
Pyridine–Pyridine <sup>g</sup>	45.6	44.1	49.6; 47.8

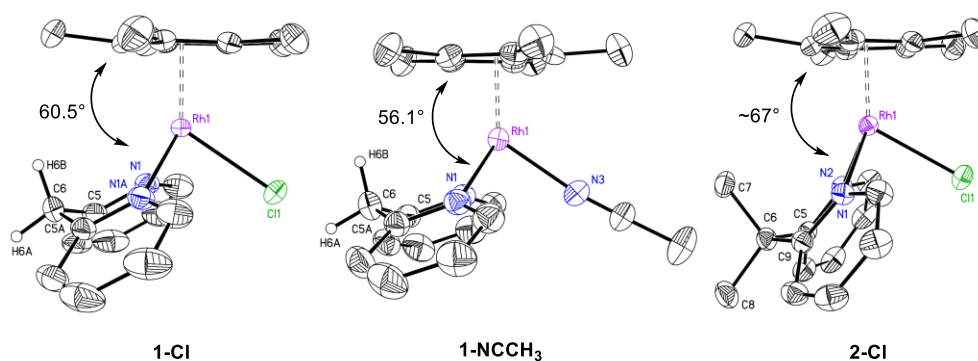
<sup>a</sup> Values for two independent molecules in the asymmetric unit cell listed. <sup>b</sup> Rh1–N2 distances. <sup>c</sup> Distance between Rh and the centroid of the Cp\* ring. <sup>d</sup> N1–Rh1–N2 angles. <sup>e</sup> C5–C6–C9 angles. <sup>f</sup> Angle between the plane defined by the Cp\* ring and the plane defined by Rh and the two pyridine N atoms. <sup>g</sup> Angle between the planes defined by the two pyridine rings in the bidentate ligand.

Comparison of the structural metrics of complexes **1-Cl** and **1-NCCH<sub>3</sub>** with that of **2-Cl** (Table 1) is useful in assessing the effects of the lack of methylation at the bridging position on the coordination behavior of the dpma ligand. As previously reported,<sup>19</sup> the  $\text{Me}_2\text{dpma}$  ligand binds to the  $[\text{Cp}^*\text{Rh}]$  fragment in similar fashion to its non-methylated analogue—via its two N donors—although the complex crystallizes in a different space group (*P*-1). Due to the six-membered metallocycle in **2-Cl**, analogous to that in **1-Cl** and **1-NCCH<sub>3</sub>**, the bite angle of the  $\text{Me}_2\text{dpma}$  ligand is significantly larger than that displayed by bpy ( $85.44(8)^\circ$  and  $85.58(8)^\circ$ , respectively, for the two independent Rh complexes in the asymmetric unit cell of **2-Cl**), similar to that displayed by dpma platform in **1-Cl** and **1-NCCH<sub>3</sub>**. On the other hand, methylation of the bridging position has a much more substantial effect on the orientation of the bidentate ligand with respect to the  $[\text{Cp}^*\text{Rh}]$  fragment. In **1-Cl**, the angle between the plane defined by the five ring carbon atoms of the Cp\* ligand and the plane defined by Rh1, N1, and N1A—a measure of the orientation of the bidentate ligand relative to the  $[\text{Cp}^*\text{Rh}]$  fragment—is  $60.5^\circ$ . In **2-Cl**, the  $\text{Me}_2\text{dpma}$  ligand is bent further away from the Cp\* fragment, with the corresponding angles being  $67.4^\circ$  and  $66.8^\circ$ , respectively, for the two independent molecules in the asymmetric unit cell (Figure 3). This observation is explained by the presence of significant steric clash in **2-Cl** between  $[\text{Cp}^*]$  and the upward-facing methyl group on the ligand bridging position. In the dpma analogue **1-Cl**, this steric interaction is absent due to the lack of methyl groups on C6. Consequently, the bidentate fragment is found to adopt an orientation that is more similar to that of bpy, which is also sterically unhindered due to the planar five-membered metallocycle enforced by the conjugated ligand (cf.  $\sim 59^\circ$  angle between  $[\text{Cp}^*]$  and bpy planes).<sup>39,40</sup> Notably, exchange of  $\text{Cl}^-$  for  $\text{CH}_3\text{CN}$  results in further narrowing of the angle between the bidentate scaffold and the Cp\* ligand ( $56.1^\circ$  in **1-NCCH<sub>3</sub>**). This observation is likely a consequence of the contraction of the Rh–N<sub>NCMe</sub> bond ( $2.080(4)$  Å) with respect to the Rh–Cl bond in **1-Cl** ( $2.4078(8)$  Å), which results in greater

steric crowding at Rh and causes the bidentate platform to be pushed further towards the Cp\* fragment.

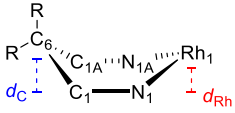
The consequences of steric clash between backbone methyl groups of Me<sub>2</sub>dpma and the Cp\* ligand are also evident from differences in the conformations of the six-membered metallocycles in complexes **1-L** and **2-Cl**. While none of these metallocycles is planar, and all adopt a boat-like conformation—i.e., the Rh center and the bridging carbon (C6) are on the same side of the plane at the base of the “boat,” defined by the two nitrogen and two *ortho*-carbon atoms (Table 2)—the respective deviations from planarity are significantly

different. In **2-Cl**, Rh1 is located ca. 0.45 Å from this plane, while the distance of the plane to C6 is ca. 0.64 Å. Because of the change in orientation of the bidentate platform with respect to the [Cp\*Rh] fragment, the corresponding distortions in **1-Cl** are substantially different, with Rh1 and C6 located 0.79 and 0.57 Å, respectively, from the N1-C5-C5A-N1A plane. Notably, rotation of the dpma ligand in **1-NCCH<sub>3</sub>** toward Cp\* further exacerbates these distortions, with Rh1 located further away from the boat plane (0.94 Å) and C6 located closer to the same plane (0.54 Å) than in either **1-Cl** or **2-Cl**.



**Figure 3.** Comparison of the solid-state structures of complexes **1-Cl** (left), **1-NCCH<sub>3</sub>** (middle), and **2-Cl** (right) highlighting the orientation of the bidentate bis(pyridine) ligand framework relative to the Cp\* motif as a function of ligand substitution and identity of monodentate ligand (Cl<sup>−</sup> vs. CH<sub>3</sub>CN).

**Table 2.** Selected structural parameters in six-membered metallocycles in **1-L** and **2-Cl** complexes.

			
	<b>1-Cl</b> (R=H)	<b>1-NCCH<sub>3</sub></b> (R=H)	<b>2-Cl</b> (R=CH <sub>3</sub> ) <sup>a</sup>
$d_C$	0.57 Å	0.54 Å	0.64 Å
$d_{Rh}$	0.79 Å	0.94 Å	0.45 Å

<sup>a</sup> Average value from two independent molecules in the asymmetric unit cell.

Thus, despite their similar structural features, complexes of the dpma and Me<sub>2</sub>dpma ligands display key differences as a consequence of ligand methylation. In particular, steric clash between the bulky Cp\* and methyl groups on the bis(pyridyl) framework affects the binding orientation of the bidentate ligand as well as the distortions of the six-membered metallocycles enforced by these platforms. These variations appear to be sufficiently significant to result in changes in the reactivity profile of these species as observed in the qualitative relative rates of Cl<sup>−</sup> abstraction in **1-Cl** vs. **2-Cl**.

### Electrochemistry

The effects of the absence of methylation on the dpma backbone on the properties of its [Cp\*Rh] complexes were further studied by electrochemical methods. Cyclic voltammograms (CVs) of complex **1-Cl** in CH<sub>3</sub>CN (see Figure S15 in ESI) reveal a complex profile, with multiple irreversible

electron transfer (ET) events. In cathodic scans starting at positive potentials (>0.5 V vs. the ferrocenium/ferrocene couple, hereafter denoted as Fc<sup>+/0</sup>), a first set of reduction events was observed near −1.5 V vs. Fc<sup>+/0</sup>; further scanning reveals additional reduction events between −1.6 and −2 V vs. Fc<sup>+/0</sup>. On the return anodic scans, multiple oxidation events are observed between −1.5 and +0.5 vs. Fc<sup>+/0</sup>. Furthermore, sequential scans display different features (see Figure S16 in ESI), suggesting that electron transfer in solution leads to generation of multiple species and/or modification of the electrode surface.

These observations are consistent with the electrochemical behavior of **2-Cl**, which likewise displays a complex profile in cyclic voltammetry experiments. In complex **2-Cl**, the presence of a coordinating Cl<sup>−</sup> counteranion has a deleterious effect on the electrochemical behavior of the [Cp\*Rh(Me<sub>2</sub>dpma)]<sup>2+</sup> system due to generation of the known Rh(II) dimer [Cp\*RhCl]<sub>2</sub> upon initial 1e<sup>−</sup> reduction.<sup>19,41,42</sup> On the other hand, electrochemical studies carried out on the solvento complex **2-CH<sub>3</sub>CN** (in the explicit absence of Cl<sup>−</sup>) reveal the rich electrochemical profile of this system, masked in other experiments by Cl<sup>−</sup>-promoted degradation of reduced material produced *in situ*. On the basis of these observations, we hypothesized that Cl<sup>−</sup> could play a similar role in complex **1-Cl**, and therefore undertook electrochemical characterization of **1-NCCH<sub>3</sub>**.

CVs of **1-NCCH<sub>3</sub>** (Figure 4) reveal a quasireversible reduction event centered at −1.10 V vs. Fc<sup>+/0</sup> ( $\Delta E_p \approx 95$  mV, similar to Fc<sup>+/0</sup> under our conditions); at more negative potentials (< −1.6 V vs. Fc<sup>+/0</sup>) a set of broad, irreversible reductions are observed, giving rise to several anodic features (see Figure S18 in ESI). The event



at  $-1.10$  V is consistent with  $1e^-$  reduction of **1-NCCH<sub>3</sub>** to a rhodium(II) species due to marked similarity with the Rh(III/II) couple in **2-NCCH<sub>3</sub>**,<sup>19</sup> as well as with the potentials required for initial reduction of other [Cp\*Rh] complexes supported by other  $\alpha$ -diimine ligands.<sup>14-17,43</sup> Furthermore, the pyridine fragments of the dpma ligand are likely redox-inactive at these potentials,<sup>44</sup> further corroborating the assignment of the observed process as a Rh-centered event. However, the rhodium(III/II) couple in the present system is observed at a significantly more negative potential ( $\Delta E_{1/2} = 0.25$  V) than the corresponding process in **2-NCCH<sub>3</sub>** ( $E_{1/2} = -0.85$  V vs.  $Fc^{+/0}$ ; Figure 5), indicating **1-NCCH<sub>3</sub>** is a significantly weaker oxidant than its Me<sub>2</sub>dpma-supported analogue. The structural changes engendered by substitution of Cl<sup>-</sup> with CH<sub>3</sub>CN in complex **1-L**, whereby the bidentate ligand adopts a different orientation may explain the observed difference in reduction potential; the narrowing of the angle between the bidentate platform and the Cp\* ring may improve overlap between bis(pyridyl) donor orbitals and orbitals on Rh, resulting in stronger bonding and in a consequently more electron-rich Rh center. Although a solid-state structure for **2-NCCH<sub>3</sub>** is not available, and direct comparison of the bond metrics for the two complexes used in electrochemical studies is therefore not possible, we tentatively propose that an analogous reorientation of the bidentate ligand in **2-NCCH<sub>3</sub>** would be hindered by the backbone methyl substituents, thereby resulting in the observed positive shift in potential for the corresponding Rh(III/II) couple. Alternatively, binding of CH<sub>3</sub>CN to Rh in **2-NCCH<sub>3</sub>** may be hindered by the more sterically hindering methylated backbone, which would result in decreased electron density at Rh and, consequently, in a more positive Rh(III/II) reduction potential for the complex supported by the methylated backbone. Notably, this rationale is supported by the slightly elongated Rh–Cl distances in **2-Cl** vs. **1-Cl** (Table 1).

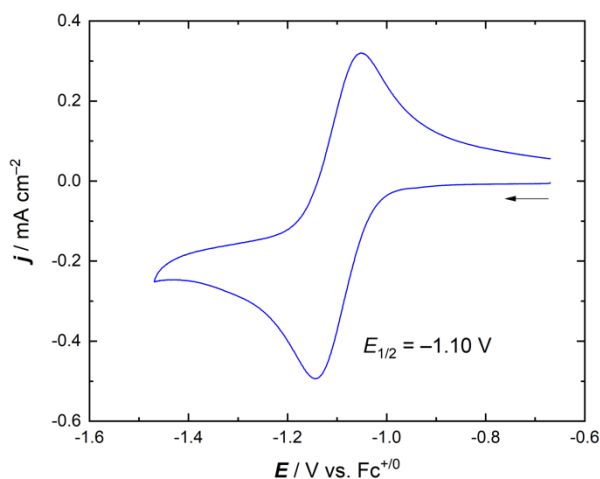


Figure 4. CV data (CH<sub>3</sub>CN, 0.1 M [nBu<sub>4</sub>N][PF<sub>6</sub>]) for **1-NCCH<sub>3</sub>**.

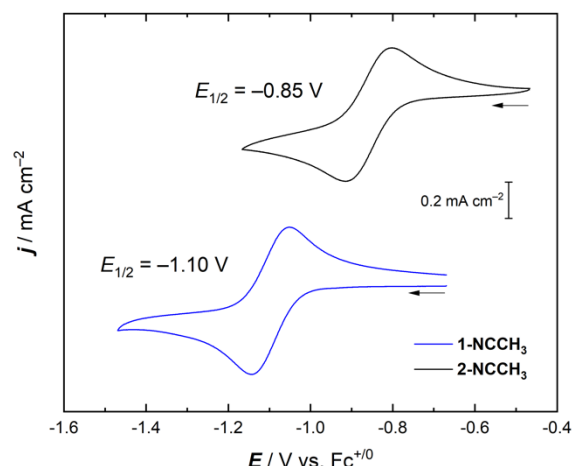


Figure 5. CV data (CH<sub>3</sub>CN, 0.1 M [nBu<sub>4</sub>N][PF<sub>6</sub>]) for **1-NCCH<sub>3</sub>** (blue line) and **2-NCCH<sub>3</sub>** (black line).

The observation of multiple reductive and oxidative events following the initial, quasireversible  $1e^-$  reduction indicates that introduction of further electron equivalents to the nascent Rh(II) complex results in substantial speciation. This finding stands in stark contrast with the electrochemically irreversible ( $E_{pc} = -1.50$  V,  $E_{pa} = -1.02$  V vs.  $Fc^{+/0}$ ) but chemically reversible  $1e^-$  process corresponding to generation of a stable rhodium(I) complex in **2-NCCH<sub>3</sub>**. Thus, while  $2e^-$  reduction of **2-NCCH<sub>3</sub>** results in formation of a stable, formally Rh(I) complex in which one of the pyridine groups of the Me<sub>2</sub>dpma ligand is facially bound to Rh via its aromatic  $\pi$ -system, double reduction of **1-NCCH<sub>3</sub>** results in degradation of the complex. These observations indicate that methylation of the bis(pyridyl) backbone is crucial to enabling access to highly-reduced species on these platforms.

Furthermore, potential cycling within the potential window of the quasireversible rhodium(III/II) couple in **1-NCCH<sub>3</sub>** results in gradual changes to the CV profile (see Figure S21 in ESI). These changes in the voltammetric response suggest that the  $1e^-$  reduced complex may be unstable at timescales longer than that of a single CV experiment; a lack of any detectable degradation in the related electrochemical data for **2-NCCH<sub>3</sub>** supports a role for the backbone methyl groups in stabilizing the electron-rich reduced metal center as we have previously discussed.<sup>19</sup>

### Chemical Reactivity Studies

On the basis of the observed electrochemical profile of complexes **1-L**, we next endeavored to study the chemical reduction of these species in order to provide evidence for assignment of the various reduction processes observed in CV experiments. In particular,  $1e^-$  reduction of **1-NCCH<sub>3</sub>** was targeted to conclusively identify the putative Rh(II) complex analogous to [Cp\*Rh<sup>II</sup>(Me<sub>2</sub>dpma)]<sup>+</sup>, and addition of multiple reducing equivalents was studied to assess the fate of the complex upon degradation. These investigations provide further insight into the consequences of methylation at the bridging methylene position in these bis(pyridyl) scaffolds and their [Cp\*Rh] complexes.

Treatment of **1-NCCH<sub>3</sub>** with a slightly substoichiometric (0.95 equiv.) amount of cobaltocene ( $\text{Cp}_2\text{Co}$ ,  $E_{1/2} = -1.34$  V vs.  $\text{Fc}^{+/0}$ )<sup>45</sup> in a THF/ $\text{CH}_3\text{CN}$  mixture results in a color change from yellow to dark purple. Removal of volatiles *in vacuo* and analysis of the dark-colored residue by NMR reveals the appearance of cobaltocenium ( $[\text{Cp}_2\text{Co}]^+$ ,  $\delta$  5.67 ppm;<sup>46</sup> see Figure S11 in ESI) as the primary diamagnetic component of the product mixture. Concurrently, disappearance of the signals associated with **1-NCCH<sub>3</sub>** indicate conversion of the diamagnetic starting material to a paramagnetic compound. A set of broad peaks was observed at 16–18 ppm, consistent with paramagnetically shifted resonances associated with a one-electron reduced complex (see Figure S11 in ESI). Additionally, multiple minor diamagnetic resonances ( $\leq 10\%$  vs.  $[\text{Cp}_2\text{Co}]^+$ ) were observed in the aromatic and aliphatic regions, indicating the possible presence of degradation products in agreement with the partial degradation observed during electrochemical experiments (*vide supra*). Attempts to cleanly isolate the putative Rh(II) species generated upon reduction (**3**, Scheme 1) were unsuccessful due to the similar solubility profiles of all components in the product mixture. Likewise, attempts to obtain single crystals suitable for XRD have not been successful. Therefore, we turned to electron paramagnetic resonance (EPR) spectroscopy to probe the identity of the paramagnetic product(s).

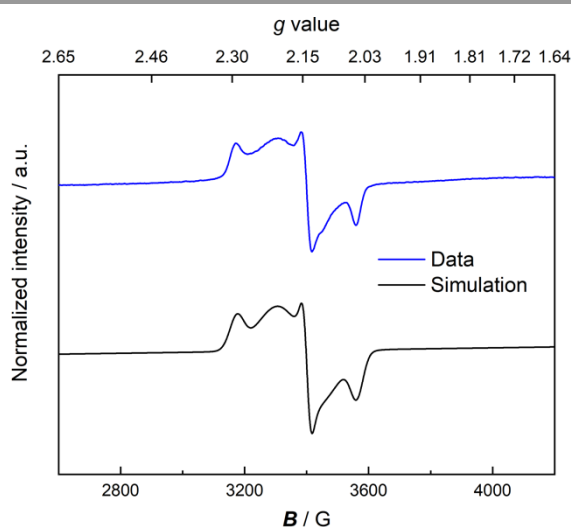


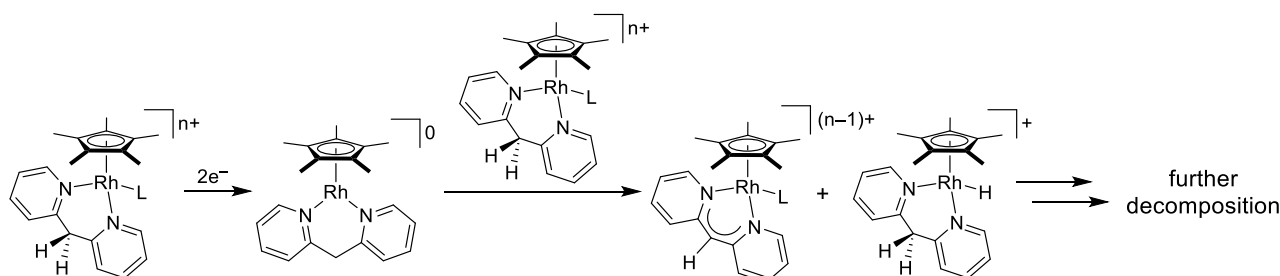
**Figure 6.** Blue line: perpendicular-mode X-band EPR spectrum of the product of reduction of **1-NCCH<sub>3</sub>** with  $\text{Cp}_2\text{Co}$  (3:1 toluene/ $\text{CH}_3\text{CN}$ , 10 K, frequency = 9.64077 GHz, power = 2 mW). Black line: Easyspin simulation of EPR data (see ESI for simulation parameters).

EPR data for this material obtained at 10 K in a frozen 3:1 toluene/ $\text{CH}_3\text{CN}$  mixture reveal a complex signal near  $g = 2$  (Figure 6). The experimental data was modelled using the Easyspin<sup>47</sup> package in MATLAB, and was best fit as a two-component mixture: component **A** displays a rhombic signal ( $g_x = 2.17$ ,  $g_y = 2.03$ ,  $g_z = 1.93$ ) with small hyperfine coupling to the

$I = 1/2$   $^{103}\text{Rh}$  nucleus; component **B**, on the other hand, displays an isotropic ( $g = 2.04$ ) signal broadened by significant unresolved hyperfine couplings. The ratio of the two components obtained from the fitting program was **A:B** = 1.2/1 (see Figure S20 in ESI for further modelling parameters). The rhombic signal observed for component **A** is consistent with a Rh-centered radical as expected for Rh(II) complex **3** (Scheme 1), analogous to the Rh(II) complex generated by  $1e^-$  reduction of **2-NCCH<sub>3</sub>**, for which we have previously reported conclusive assignment via structural characterization by XRD. EPR signatures similar to that observed for component **A** in the present work have been reported for literature complexes featuring Rh centers in the unusual +II oxidation state.<sup>48–54</sup> However, we note here that, in the absence of structural data, retention or loss of the Rh-bound  $\text{CH}_3\text{CN}$  solvent molecule in **3** cannot be conclusively established. The Rh(II) complex supported by the  $\text{Me}_2\text{dpma}$  platform is a  $17e^-$  species in which the  $\text{CH}_3\text{CN}$  ligand is absent; however, the differences in binding profile between dpma and  $\text{Me}_2\text{dpma}$  and in the propensity of the complexes of these ligands to undergo ligand exchange (*vide supra*) may favor generation of a  $19e^-$  species in this case. The observation of a signal for a second paramagnetic species indicates that degradation can occur during reduction of **1-NCCH<sub>3</sub>**, corroborating the electrochemical data. The broad appearance of this signal supports its assignment as a metal-based radical rather than organic radical species. However, in the absence of additional structural information, the identity of component **B** cannot be conclusively determined. Therefore, on the basis of these EPR data, we conclude that  $1e^-$  reduction of **1-NCCH<sub>3</sub>** results in generation of Rh(II) complex **3** (component **A** in the EPR spectrum), indicating that the dpma platform can support a Rh(II) center, even in the absence of stabilizing interactions with backbone C–H bonds. On the other hand, the observation of multiple paramagnetic components in the product mixture implicates generation of multiple products during reduction of **1-NCCH<sub>3</sub>**.

As electrochemical experiments indicate that reduction of **3** is accompanied by substantial follow-up chemical reaction steps, further chemical reduction experiments were undertaken to provide insight into the possible product(s) of these chemical processes. Treatment of a tetrahydrofuran (THF) suspension of **1-Cl** with excess sodium-mercury amalgam ( $\text{Na}(\text{Hg})$ , a common reagent for preparation of highly-reduced Rh half-sandwich complexes<sup>38,55</sup>) results in a moderately rapid ( $\sim 30$  min) change in color from yellow-orange to dark purple, as well as generation of a more homogeneous reaction solution. Analysis of the reaction mixture by spectroscopic methods was carried out following filtration of the reaction mixture to remove excess  $\text{Na}(\text{Hg})$  and  $\text{Na}^+$  salts and removal of volatile materials *in vacuo*. The resulting dark purple residue was no longer soluble in polar solvents such as  $\text{CH}_3\text{CN}$ , indicating a substantial change in the overall charge of the species, consistent with reduction, as observed in analogous literature complexes.<sup>14,16,19</sup>

## ARTICLE



**Scheme 2.** Proposed decomposition pathway via electron and proton transfer steps.

The  $^1\text{H}$  NMR spectrum of the dark purple material in  $d_6$ -benzene ( $\text{C}_6\text{D}_6$ ) indicates generation of multiple new species (Figure S12 in ESI); two resonances were observed in the region near 1.86 ppm, suggesting the presence of multiple  $\text{Cp}^*$  environments, and thus multiple  $[\text{Cp}^*\text{Rh}]$  products, as well as some free (i.e. not Rh-bound) dpma ligand. In accordance with this assignment, multiple sets of pyridine resonances were observed in the aromatic region. Attempts to separate the multiple components were unsuccessful, and subsequent  $^1\text{H}$  NMR experiments revealed substantial decomposition of the initial mixture over time, making assignment of the identity of the two reduced products challenging. (See Figure S12 in ESI for all spectra discussed here).

Treatment of **1-Cl** with  $\text{Na}(\text{Hg})$  for longer times (2–16 hours) engenders a further color change from dark purple to brown.  $^1\text{H}$  NMR analysis following workup indicated a significantly more complex mixture than that observed at shorter reaction times, indicating substantial decomposition following delivery of additional reducing equivalents. However, a signal observed at  $-14.6$  ppm in the NMR of this mixture is consistent with generation of a metal–hydride species, providing a key insight into the identity of one of the products of the double reduction of **1-Cl**.

Given the known deleterious effects of  $\text{Cl}^-$  on the  $1e^-$  reduction of both **1-Cl** (on the basis of its electrochemical behavior, *vide supra*) and **2-Cl** (on the basis of both electrochemical and chemical evidence),<sup>19</sup> we additionally attempted double reduction of **1-NCCH<sub>3</sub>** to determine whether Rh(I) compounds could be cleanly isolated via this route. Treatment of **1-NCCH<sub>3</sub>** with 1.9 equiv.  $\text{Cp}^*\text{Co}_2$  ( $E_{1/2} = -1.91$  V vs.  $\text{Fc}^{+/0}$ )<sup>45</sup> in  $\text{CH}_3\text{CN}$ /tetrahydrofuran (THF) results in a change in color from bright yellow to brown. After 1 h, the volatiles were removed *in vacuo*, and the residue extracted with hexanes. This solution was filtered, and the solvent was evaporated to give a red-brown material.  $^1\text{H}$  NMR analysis revealed a complex mixture of compounds as indicated by the intricate aromatic and aliphatic regions, and generation of a substantial amount of free dpma ligand (see Figure S13 in the ESI). Additionally, signals in the

traditional metal–hydride region ( $-8$  to  $-12$  ppm) were observed, indicating partial generation of metal-protonated species, as well as several peaks with substantial downfield shifts (15 to 65 ppm), suggesting formation of paramagnetic compounds.

Despite the complex mixtures obtained in attempts at double reduction of Rh(III) complexes **1-Cl** and **1-NCCH<sub>3</sub>**, the observation of metal–hydride species provides key evidence on of the products of the chemical reaction steps accessible to reduced forms of **1-L** (see Figure S12 in ESI). Reduction of **1-L** to a rhodium(I) species can be reasonably expected to significantly increase the basicity of the metal complex—rhodium(I) complexes supported by various bidentate ligands are well known to undergo protonation with mild organic acids (e.g.  $[\text{Et}_3\text{NH}]^+$ ,  $\text{p}K_a = 18.9$  in  $\text{CH}_3\text{CN}$ ).<sup>13,14,56</sup> Furthermore, interaction between the rhodium(II) center supported by the  $\text{Me}_2\text{dpma}$  framework and a backbone methyl C–H bond can be attributed to significant basicity of the metal center ( $E_{\text{pc}}(\text{Rh}^{\text{II}}/\text{Rh}^{\text{I}}) \approx -1.5$  V vs.  $\text{Fc}^{+/0}$ ).<sup>19</sup>

However, unlike previously studied bidentate platforms, the dpma ligand possesses two doubly benzylic C–H bonds on the inter-ring bridging methylene group. These are likely to be sufficiently acidic (cf., the  $\text{p}K_a$  of the benzylic proton in 9-CN-fluorene, 21.4 in  $\text{CH}_3\text{CN}$ )<sup>56</sup> to protonate nascent reduced species. Furthermore, we note that the binding of dpma to rhodium(III), as in **1**, likely further increases the acidic nature of these protons. In agreement with this interpretation of the observed data, deprotonation of the methylene bridging position of a boron-bound dpma ligand by free dpma has been reported.<sup>20</sup>

On the basis of the observed NMR and electrochemical data, a plausible pathway to explain conversion of **1-L** into multiple species upon reduction can be formulated (Scheme 2). Initial generation of a rhodium(I) species from **1-L**, in the presence of residual rhodium(III) complex, could lead to partial protonation of the reduced complex(es) by **1-L**. The deprotonated **1-L**, now supported by an anionic LX-type ligand, could then undergo subsequent reduction leading to further decomposition. Based



on the intractable mixtures obtained from chemical reduction experiments, it is apparent that the protonated species supported by the dpma ligand are also unstable, a clear departure from the stability of the protonated complexes—including both  $[\text{Cp}^*\text{H}]$  and  $[\text{Rh}-\text{H}]$  species—supported by other bidentate ligands.<sup>13,16,17</sup>

### 3. Conclusions

Half-sandwich rhodium complexes of the bis(pyridyl) dpma ligand have been prepared and characterized by spectroscopic, structural, and electrochemical methods. The absence of methylation at the bridging methylene position in this platform vs. its previously reported  $\text{Me}_2\text{dpma}$  analogue has substantial effects on the properties and reactivity profile of  $[\text{Cp}^*\text{Rh}]$  complexes. *In primis*, while both ligands enforce a six-membered metallocycle that results in a wider bite angle than those enforced by other common bidentate ligands, the less bulky dpma ligand can twist further towards the  $\text{Cp}^*$  ligand than its more sterically hindered analogue. Though subtle, this change appears to have a significant effect on the relative reactivity of the two complexes, as the qualitative rate of chloride abstraction is much slower for dpma-supported complex **1-Cl** than  $\text{Me}_2\text{dpma}$  complex **2-Cl**.

Electrochemical studies in the absence of chloride reveal that solvento complex **1-NCCH<sub>3</sub>** undergoes a quasireversible one-electron reduction at  $-1.10$  V vs.  $\text{Fc}^{+/0}$ . In accord with this finding, chemical reduction experiments with  $\text{Cp}_2\text{Co}$  suggest generation of rhodium(II) complex **3** as part of a mixture of paramagnetic species. This behavior closely resembles that of the complexes of the  $\text{Me}_2\text{dpma}$  ligand, although both electrochemical and chemical experiments also indicate significant degradation during reduction in the dpma reactivity described here. Additionally, the change in substitution on the ligand scaffolds also results in a substantial (250 mV) shift to more negative potential for the  $\text{Rh}(\text{III}/\text{II})$  reduction of the dpma-ligated **1-NCCH<sub>3</sub>**, underscoring the significance of the change in ligand orientation engendered by the unsubstituted bridging methylene group.

Electrochemically, initial  $1e^-$  reduction of **1-NCCH<sub>3</sub>** is followed by multiple irreversible reductive processes consistent with chemical reactivity that follows transfer of additional reducing equivalents. Chemical reduction experiments to investigate these follow-up reactions reveal substantial degradation, including generation of at least one metal-hydride species as observed via  $^1\text{H}$  NMR. These observations can be readily rationalized by the presence of two doubly benzylic protons on the bridging methylene group of the dpma scaffold—upon generation of highly basic reduced species beyond rhodium(II), deprotonation of the dpma scaffold on a second rhodium complex (Scheme 2) can occur. This behavior stands in stark contrast with that of the analogous  $\text{Me}_2\text{dpma}$  complexes, in which reduction to a formally rhodium(I) complex is enabled by rearrangement of the bis(pyridyl) ligand to bind to the Rh center via the  $\pi$  system of one of its pyridine rings. Thus, the observed participation of the dpma ligand scaffold in  $\text{H}^+$ -transfer reactivity highlights the importance of the absence of acidified

benzylic protons in the design of ligand platforms to support reducing, and thus relatively basic, half-sandwich complexes.

## 4. Experimental Section

### General Considerations

All manipulations were carried out in dry  $\text{N}_2$ -filled gloveboxes (Vacuum Atmospheres Co., Hawthorne, CA) or under  $\text{N}_2$  atmosphere using standard Schlenk techniques unless otherwise noted. All solvents were of commercial grade and dried over activated alumina using a PPT Glass Contour (Nashua, NH) solvent purification system prior to use, and were stored over molecular sieves. All chemicals were from major commercial suppliers and used as received after extensive drying.  $[\text{Cp}^*\text{RhCl}_2]_2$  and dpma were prepared according to literature procedures.<sup>37,57,58</sup>  $\text{CD}_3\text{CN}$  was purchased from Cambridge Isotope Laboratories and dried over 3-Å molecular sieves.  $^1\text{H}$ ,  $^{13}\text{C}$ ,  $^{19}\text{F}$ , and  $^{31}\text{P}$  NMR spectra were collected on 400 or 500 MHz Bruker spectrometers and referenced to the residual protio-solvent signal<sup>59</sup> in the case of  $^1\text{H}$  and  $^{13}\text{C}$ . Heteronuclear NMR spectra were referenced to the appropriate external standard following the recommended scale based on ratios of absolute frequencies ( $\Xi$ ).<sup>60,61</sup>  $^{19}\text{F}$  NMR spectra are reported relative to  $\text{CCl}_3\text{F}$ , and  $^{31}\text{P}$  NMR spectra are reported relative to  $\text{H}_3\text{PO}_4$ . Chemical shifts ( $\delta$ ) are reported in units of ppm and coupling constants ( $J$ ) are reported in Hz. Electronic absorption spectra were collected with an Ocean Optics Flame spectrometer, in a 1 cm pathlength quartz cuvette. Elemental analyses were performed by Midwest Microlab (Indianapolis, IN).

### Electrochemistry

Electrochemical experiments were carried out in a nitrogen-filled glove box. 0.10 M tetra(n-butylammonium) hexafluorophosphate (Sigma-Aldrich; electrochemical grade) in acetonitrile served as the supporting electrolyte. Measurements were made with a Gamry Reference 600 Plus Potentiostat/Galvanostat using a standard three-electrode configuration. The working electrode was the basal plane of highly oriented pyrolytic graphite (HOPG, GraphiteStore.com, Buffalo Grove, Ill.; surface area:  $0.09\text{ cm}^2$ ), the counter electrode was a platinum wire (Kurt J. Lesker, Jefferson Hills, PA; 99.99%, 0.5 mm diameter), and a silver wire immersed in electrolyte served as a pseudo-reference electrode (CH Instruments). The reference was separated from the working solution by a Vycor frit (Bioanalytical Systems, Inc.). Ferrocene (Sigma Aldrich; twice-sublimed) was added to the electrolyte solution at the conclusion of each experiment ( $\sim 1\text{ mM}$ ); the midpoint potential of the ferrocenium/ferrocene couple (denoted as  $\text{Fc}^{+/0}$ ) served as an external standard for comparison of the recorded potentials. Concentrations of analyte for cyclic voltammetry were typically 2 mM.

### Synthetic Procedures

**Synthesis of 1-Cl.** To a suspension of  $[\text{Cp}^*\text{RhCl}_2]_2$  (0.6688 g, 1.08 mmol) in 5 mL acetonitrile ( $\text{CH}_3\text{CN}$ ) were added dpma (0.3684

g, 2.16 mmol, 2 equiv) and  $\text{AgPF}_6$  (0.5472 g, 2.16 mmol, 2 equiv) as  $\text{CH}_3\text{CN}$  solutions. The color of the reaction mixture rapidly changed from brick-red to yellow-orange, and a colorless precipitate formed. After 30 min, the suspension was filtered to remove the  $\text{AgCl}$  byproduct, and the volume of the filtrate was reduced to ca. 5 mL. Addition of diethyl ether ( $\text{Et}_2\text{O}$ , 20 mL) caused precipitation of a yellow-orange solid, which was collected by filtration (1.2386 g, 97%). Single-crystals suitable for X-ray diffraction studies were obtained by vapor diffusion of  $\text{Et}_2\text{O}$  into a concentrated  $\text{CH}_3\text{CN}$  solution of the title compound.  $^1\text{H}$  NMR (500 MHz,  $\text{CD}_3\text{CN}$ ):  $\delta$  8.79 (d,  $^3J_{\text{H,H}} = 5.8$  Hz, 2H, H1), 7.98 (m, 2H, PyH), 7.69 (d,  $^3J_{\text{H,H}} = 7.9$  Hz, 2H, H4), 7.48 (m, 2H, PyH), 4.51 (d,  $^2J_{\text{H,H}} = 15.5$  Hz, 1H, H6A), 4.06 (d,  $^2J_{\text{H,H}} = 15.4$  Hz, 1H, H6B), 1.58 (s, 15H,  $\text{C}_5(\text{CH}_3)_5$ ) ppm.  $^{13}\text{C}\{^1\text{H}\}$  NMR (126 MHz,  $\text{CD}_3\text{CN}$ ):  $\delta$  157.09 (C5), 155.69 (C1), 141.28, 127.09, 125.93, 97.82 (d,  $^1J_{\text{C,Rh}} = 8.4$  Hz,  $\text{C}_5(\text{CH}_3)_5$ ), 46.69 (C6), 9.26 ( $\text{C}_5(\text{CH}_3)_5$ ) ppm.  $^{31}\text{P}\{^1\text{H}\}$  NMR (162 MHz,  $\text{CD}_3\text{CN}$ ):  $\delta$  145.48 (sept,  $^1J_{\text{P,F}} = 706.4$  Hz,  $\text{PF}_6^-$ ) ppm.  $^{19}\text{F}$  NMR (376 MHz,  $\text{CD}_3\text{CN}$ ):  $\delta$  -73.73 (d,  $^1J_{\text{F,P}} = 706.4$  Hz,  $\text{PF}_6^-$ ) ppm. Electronic absorption spectrum ( $\text{CH}_3\text{CN}$ ): 236 (19,600), 260 (11,800), 367 nm ( $2,700 \text{ M}^{-1} \text{ cm}^{-1}$ ). Anal. Calcd. for  $\text{C}_{21}\text{H}_{25}\text{ClF}_6\text{N}_2\text{PRh}$ : C, 42.84, H, 4.28, N, 4.76 %; Found: C, 43.02, H, 3.99, N, 5.07 %.

**Synthesis of 1-NCCH<sub>3</sub>.** To a solution of 1-Cl (0.0728 g, 0.124 mmol) in  $\text{CH}_3\text{CN}$  (5 mL) was added a solution of  $\text{AgPF}_6$  (0.0313 g, 0.124 mmol, 1 equiv.) in  $\text{CH}_3\text{CN}$ . The reaction vessel was sealed and covered with aluminium foil, and the reaction mixture was stirred in the dark for 3 days. After 3 days, a colorless precipitate had formed, which was filtered off. Volatiles were removed from the filtrate *in vacuo* to obtain 1-NCCH<sub>3</sub> as a yellow foamy solid in quantitative yield. Single-crystals suitable for X-ray diffraction studies were obtained by vapor diffusion of  $\text{Et}_2\text{O}$  into a concentrated  $\text{CH}_3\text{CN}$  solution of the title compound.  $^1\text{H}$  NMR (500 MHz,  $\text{CD}_3\text{CN}$ ):  $\delta$  8.74 (dd,  $^3J_{\text{H,H}} = 5.7$ ,  $^4J_{\text{H,H}} = 1.6$  Hz, 2H, H1), 8.10 (m, 2H, PyH), 7.81 (d,  $^3J_{\text{H,H}} = 7.8$  Hz, 2H, H4), 7.61 (t,  $^3J_{\text{H,H}} = 6.8$  Hz, 2H, PyH), 4.63 (d,  $^2J_{\text{H,H}} = 15.8$  Hz, 1H, H6A), 3.91 (d,  $^2J_{\text{H,H}} = 15.7$  Hz, 1H, H6B), 1.63 (s, 15H,  $\text{C}_5(\text{CH}_3)_5$ ) ppm.  $^{13}\text{C}\{^1\text{H}\}$  NMR (126 MHz,  $\text{CD}_3\text{CN}$ ):  $\delta$  156.83 (C5), 154.61 (C1), 142.32, 128.40, 127.09, 100.85 (d,  $^1J_{\text{C,Rh}} = 8.2$  Hz,  $\text{C}_5(\text{CH}_3)_5$ ), 46.70 (C6), 9.36 ( $\text{C}_5(\text{CH}_3)_5$ ) ppm.  $^{31}\text{P}\{^1\text{H}\}$  NMR (162 MHz,  $\text{CD}_3\text{CN}$ ):  $\delta$  -144.61 (sept,  $^1J_{\text{P,F}} = 706.6$  Hz,  $\text{PF}_6^-$ ) ppm.  $^{19}\text{F}$  NMR (376 MHz,  $\text{CD}_3\text{CN}$ ):  $\delta$  -72.88 (d,  $^1J_{\text{F,P}} = 706.4$  Hz,  $\text{PF}_6^-$ ) ppm. Electronic absorption spectrum ( $\text{CH}_3\text{CN}$ ): 237 (20,400), 261 (8,500), 347 nm ( $3,300 \text{ M}^{-1} \text{ cm}^{-1}$ ). Anal. Calcd. for  $\text{C}_{23}\text{H}_{28}\text{F}_{12}\text{N}_2\text{P}_2\text{Rh}$ : C, 37.37, H, 3.82, N, 5.68 %; Found: C, 37.08, H, 3.61, N, 5.58 %.

## Conflicts of interest

There are no conflicts to declare.

## Acknowledgements

The authors thank Dr. Justin Douglas and Sarah Neuenswander for assistance with NMR spectroscopy, and Melissa Denler for assistance with EPR spectroscopy. This work was supported by the US National Science Foundation through award OIA-

1833087. The authors also acknowledge the US National Science Foundation and US National Institutes of Health for support of the EPR instrumentation (CHE-0946883), NMR instrumentation (S10OD016360, S10RR024664, and CHE-0320648), and X-ray diffractometers (CHE-0079282 and CHE-0923449) used in this study.

## References

- N. S. Lewis and D. G. Nocera, *Proc. Natl. Acad. Sci. USA*, 2006, **103**, 15729-15735.
- W. T. Eckenhoff and R. Eisenberg, *Dalton Trans.*, 2012, **41**, 13004-13021.
- J. R. McKone, S. C. Marinescu, B. S. Brunschwig, J. R. Winkler and H. B. Gray, *Chem. Sci.*, 2014, **5**, 865-878.
- P. S. Wagenknecht, J. M. Penney and R. T. Hembre, *Organometallics*, 2003, **22**, 1180-1182.
- U. Kölle and M. Grätzel, *Angew. Chem. Int. Ed. Engl.*, 1987, **26**, 567-570.
- U. Kölle, B. S. Kang, P. Infelta, P. Comte and M. Grätzel, *Chem. Ber.*, 1989, **122**, 1869-1880.
- R. Ruppert, S. Herrmann and E. Steckhan, *Tetrahedron Lett.*, 1987, **28**, 6583-6586.
- R. Ruppert, S. Herrmann and E. Steckhan, *J. Chem. Soc. Chem. Commun.*, 1988, 1150-1151.
- R. Wienkamp and E. Steckhan, *Angew. Chem. Int. Ed. Engl.*, 1982, **21**, 782-783.
- F. Hildebrand, C. Kohlmann, A. Franz and S. Lütz, *Adv. Synth. Catal.*, 2008, **350**, 909-918.
- L. M. A. Quintana, S. I. Johnson, S. L. Corona, W. Villatoro, W. A. Goddard, M. K. Takase, D. G. VanderVelde, J. R. Winkler, H. B. Gray and J. D. Blakemore, *Proc. Natl. Acad. Sci. USA*, 2016, **113**, 6409-6414.
- C. L. Pitman, O. N. L. Finster and A. J. M. Miller, *Chem. Commun.*, 2016, **52**, 9105-9108.
- Y. Peng, M. V. Ramos-Garcés, D. Lionetti and J. D. Blakemore, *Inorg. Chem.*, 2017, **56**, 10824-10831.
- W. C. Henke, D. Lionetti, W. N. G. Moore, J. A. Hopkins, V. W. Day and J. D. Blakemore, *ChemSusChem*, 2017, **10**, 4589-4598.
- W. N. G. Moore, W. C. Henke, D. Lionetti, V. W. Day and J. D. Blakemore, *Molecules*, 2018, **23**, 2857-2874.
- E. A. Boyd, D. Lionetti, W. C. Henke, V. W. Day and J. D. Blakemore, *Inorg. Chem.*, 2019, **58**, 3606-3615.
- J. A. Hopkins, D. Lionetti, V. W. Day and J. D. Blakemore, *Organometallics*, 2019, **38**, 1300-1310.
- J. A. Hopkins, D. Lionetti, V. W. Day and J. D. Blakemore, *Unpublished results*.
- D. Lionetti, V. W. Day, B. Lassalle-Kaiser and J. D. Blakemore, *Chem. Commun.*, 2018, **54**, 1694-1697.
- P. Vasko, V. Kinnunen, J. O. Moilanen, T. L. Roemmele, R. T. Boere, J. Konu and H. M. Tuononen, *Dalton Trans.*, 2015, **44**, 18247-18259.
- M. T. Garland, J. Y. Lemarouille, E. Spodine and J. Manzur, *Acta Crystallogr., Sect. C: Cryst. Struct. Commun.*, 1986, **42**, 1720-1722.
- M. T. Garland, D. Grandjean, E. Spodine and J. Manzur, *Acta Crystallogr., Sect. C: Cryst. Struct. Commun.*, 1987, **43**, 643-645.
- E. Spodine, J. Manzur, M. T. Garland, M. Kiwi, O. Peña, D. Grandjean and L. Toupet, *J. Chem. Soc. Dalton Trans.*, 1991, 365-369.
- A. M. Garcia, J. Manzur, E. Spodine, R. F. Baggio and M. T. Garland, *Acta Crystallogr., Sect. C: Cryst. Struct. Commun.*, 1994, **50**, 1882-1884.

- 25 N. S. Sommerfeld, J. Gulzow, A. Roller, K. Cseh, M. A. Jakupc, A. Grohmann, M. Galanski and B. K. Keppler, *Eur. J. Inorg. Chem.*, 2017, 3115-3124.
- 26 M. Elie, M. D. Weber, F. Di Meo, F. Sguerra, J. F. Lohier, R. B. Pansu, J. L. Renaud, M. Hamel, M. Linares, R. D. Costa and S. Gaillard, *Chem. Eur. J.*, 2017, **23**, 16328-16337.
- 27 F. B. Zhang, C. W. Kirby, D. W. Hairsine, M. C. Jennings and R. J. Puddephatt, *J. Am. Chem. Soc.*, 2005, **127**, 14196-14197.
- 28 A. Abo-Amer, M. S. McCready, F. B. Zhang and R. J. Puddephatt, *Can. J. Chem.*, 2012, **90**, 46-54.
- 29 B. A. McKeown, H. E. Gonzalez, T. Michaelos, T. B. Gunnoe, T. R. Cundari, R. H. Crabtree and M. Sabat, *Organometallics*, 2013, **32**, 3903-3913.
- 30 B. A. McKeown, H. E. Gonzalez, T. B. Gunnoe, T. R. Cundari and M. Sabat, *ACS Catal.*, 2013, **3**, 1165-1171.
- 31 C. Mock, I. Puscasu, M. J. Rauterkus, G. Tallen, J. E. A. Wolff and B. Krebs, *Inorg. Chim. Acta*, 2001, **319**, 109-116.
- 32 J. Madureira, T. M. Santos, B. J. Goodfellow, M. Lucena, J. L. P. de Jesus, M. G. Santana-Marques, M. G. B. Drew and V. Felix, *J. Chem. Soc. Dalton Trans.*, 2000, 4422-4431.
- 33 A. J. Canty, G. Hayhurst, N. Chaichit and B. M. Gatehouse, *J. Chem. Soc. Chem. Commun.*, 1980, 316-318.
- 34 M. G. Budge, K. J. Muir, G. P. McQuillan and W. T. A. Harrison, *Crystals*, 2011, **1**, 47-58.
- 35 N. Marti, B. Spingler, F. Breher and R. Schibli, *Inorg. Chem.*, 2005, **44**, 6082-6091.
- 36 C. R. Groom, I. J. Bruno, M. P. Lightfoot and S. C. Ward, *Acta Cryst. Sect. B*, 2016, **72**, 171-179.
- 37 C. White, A. Yates and P. M. Maitlis, *Inorg. Synth.*, 1992, **29**, 228-234.
- 38 J. D. Blakemore, E. S. Hernandez, W. Sattler, B. M. Hunter, L. M. Henling, B. S. Brunschwig and H. B. Gray, *Polyhedron*, 2014, **84**, 14-18.
- 39 L. Dacsi, H. Elias, U. Frey, A. Hornig, U. Koelle, A. E. Merbach, H. Paulus and J. S. Schneider, *Inorg. Chem.*, 1995, **34**, 306-315.
- 40 M. A. Scharwitz, I. Ott, Y. Geldmacher, R. Gust and W. S. Sheldrick, *J. Organomet. Chem.*, 2008, **693**, 2299-2309.
- 41 P. R. Sharp, D. W. Hoard and C. L. Barnes, *J. Am. Chem. Soc.*, 1990, **112**, 2024-2026.
- 42 D. W. Hoard and P. R. Sharp, *Inorg. Chem.*, 1993, **32**, 612-620.
- 43 W. Kaim, R. Reinhardt, E. Waldhor and J. Fiedler, *J. Organomet. Chem.*, 1996, **524**, 195-202.
- 44 R. A. Lewis, K. C. MacLeod, B. Q. Mercado and P. L. Holland, *Chem. Commun.*, 2014, **50**, 11114-11117.
- 45 N. G. Connelly and W. E. Geiger, *Chem. Rev.*, 1996, **96**, 877-910.
- 46 S. Vanicek, H. Kopacka, K. Wurst, T. Müller, H. Schottenberger and B. Bildstein, *Organometallics*, 2014, **33**, 1152-1156.
- 47 S. Stoll and A. Schweiger, *J. Magn. Reson.*, 2006, **178**, 42-55.
- 48 M. P. Garcia, M. V. Jimenez, L. A. Oro, F. J. Lahoz, J. M. Casas and P. J. Alonso, *Organometallics*, 1993, **12**, 3257-3263.
- 49 A. Pedersen and M. Tilset, *Organometallics*, 1993, **12**, 56-64.
- 50 J. E. Collins, M. P. Castellani, A. L. Rheingold, E. J. Miller, W. E. Geiger, A. L. Rieger and P. H. Rieger, *Organometallics*, 1995, **14**, 1232-1238.
- 51 D. Menglet, A. M. Bond, K. Coutinho, R. S. Dickson, G. G. Lazarev, S. A. Olsen and J. R. Pilbrow, *J. Am. Chem. Soc.*, 1998, **120**, 2086-2089.
- 52 N. G. Connelly, D. J. H. Emslie, W. E. Geiger, O. D. Hayward, E. B. Linehan, A. G. Orpen, M. J. Quayle and P. H. Rieger, *J. Chem. Soc. Dalton Trans.*, 2001, 670-683.
- 53 C. J. Adams, N. G. Connelly, D. J. H. Emslie, O. D. Hayward, T. Manson, A. Guy Orpen and P. H. Rieger, *Dalton Trans.*, 2003, 2835-2845.
- 54 B. De Bruin, D. G. H. Hetterscheid, A. J. J. Koekkoek and H. Grützmacher, in *Progress in Inorganic Chemistry*, John Wiley & Sons, Inc., 2008, vol. 55, pp. 247-354.
- 55 H. Nakai, K. Jeong, T. Matsumoto and S. Ogo, *Organometallics*, 2014, **33**, 4349-4352.
- 56 I. Kaljurand, A. Kutt, L. Soovali, T. Rodima, V. Maemets, I. Leito and I. A. Koppel, *J. Org. Chem.*, 2005, **70**, 1019-1028.
- 57 N. Vedernikov, R. Miftakhov, S. V. Borisoglebski, K. G. Caulton and B. N. Solomonov, *Chem. Heterocycl. Compd.*, 2002, **38**, 406-416.
- 58 G. Dyker and O. Muth, *Eur. J. Org. Chem.*, 2004, 4319-4322.
- 59 G. R. Fulmer, A. J. M. Miller, N. H. Sherden, H. E. Gottlieb, A. Nudelman, B. M. Stoltz, J. E. Bercaw and K. I. Goldberg, *Organometallics*, 2010, **29**, 2176-2179.
- 60 R. K. Harris, E. D. Becker, S. M. C. De Menezes, R. Goodfellow and P. Granger, *Pure Appl. Chem.*, 2001, **73**, 1795-1818.
- 61 R. K. Harris, E. D. Becker, S. M. C. De Menezes, P. Granger, R. E. Hoffman and K. W. Zilm, *Pure Appl. Chem.*, 2008, **80**, 59-84.